Preliminary estimate of Holocene slip rate on active normal faults bounding the southern coast of the Gulf of Evia, central Greece

R.T. Walker[1], S. Claisse[1], M. Telfer[2], E. Nissen[3], P. England[1], C. Bryant[4], and R. Bailey[2]
[1]*Department of Earth Sciences, University of Oxford, Parks Road, Oxford, OX1 3PR, UK*
[2]*Oxford University Centre for the Environment, South Parks Road, Oxford, OX1 3QY, UK*
[3]*Bullard Laboratories, Cambridge University, Madingley Road, Cambridge, CB3 0EZ, UK*
[4]*NERC Radiocarbon Facility (Environment), SUERC, Rankine Avenue, East Kilbride, G75 0QF, UK*

ABSTRACT

We investigate the late Quaternary history of slip on the Kamena Vourla and Arkitsa normal faults, which are segments of a fault system bounding the south coast of the Gulf of Evia in central Greece, and which we refer to as the Coastal Fault System. We examine two river terraces, near the village of Molos, which are found within the uplifted footwall of the Kamena Vourla fault. The upper terrace is ~20 m above the present river level and appears to represent fan deposition into the main river channel from surrounding tributaries. The lower terrace, ~8 m above the present-day river bed, represents an interval of river-bed aggradation and correlates with the surface of a delta on the hanging-wall side of the fault. GPS profiles show a 6 ± 0.1 m vertical offset of the lower terrace surface as it crosses the fault. Preliminary dating of the two terrace levels, using both optical luminescence and radiocarbon methods, provides inconclusive results. The lower terrace, however, grades toward the present-day sea level and correlates with the surface of a delta on the hanging-wall side of the fault; it is, therefore, likely to date from ~6 ka, when sea level stabilized at its present-day highstand. With an age of ~6 ka, the 6 m vertical displacement of the lower terrace yields an estimate of ~1.2–2.0 mm/yr for the Holocene rate of slip across the Kamena Vourla fault. This rate of slip is comparable with an estimated rate of ~0.7–2.0 mm/yr for the central (Arkitsa) segment of the Coastal Fault System, and with a 0.4–1.6 mm/yr slip rate measured on the easternmost (Atalanti) segment. These estimates of Holocene slip rates are consistent with the 1–3 mm/yr of present-day extension across the Gulf of Evia measured by GPS, arguing against large changes in rate of extension through the Holocene. Both the Arkitsa and Kamena Vourla faults are clearly active and despite an absence of historical earthquakes on either fault, they should be considered to be a major hazard to local populations. However, further dating studies and palaeoseismic investigations are required before the slip rate and history can be fully quantified.

INTRODUCTION

Published estimates of slip rate on faults in central Greece are rare, but are important both for understanding the active tectonics of the region and for quantifying seismic hazard in this region, where population centers are concentrated in the hanging walls of the normal faults. We present a quantitative estimate of slip rate across the system of faults that bounds the southern coast of the Gulf of Evia (Fig. 1). This Coastal Fault System, comprising the Lamia, Kamena Vourla, Arkitsa, and Atalanti fault segments, is likely to accommodate the major proportion of the <3 mm/yr of geodetically measured extension across the region (see section Active Faulting in the Locris Half-graben) and therefore poses a serious hazard to local populations. There is no record of recent or historical destructive earthquakes on the Lamia, Kamena Vourla, and Arkitsa faults, and there are no quantitative estimates of their average slip rates, so the interval between earthquakes is unknown. The lack of constraint on the fault slip rates is due, at least in part, to the scarcity of suitable measurement sites within the steep, mountainous topography.

Active normal faulting in Greece has a clear geomorphic expression. The uplifted footwalls are frequently composed of resistant limestone, and large sedimentary basins form in the hanging walls (e.g., Jackson, 1994; Goldsworthy and Jackson, 2000). The two most prominent geomorphic expressions of this faulting are the Gulfs of Evia and Corinth, each of which is bounded by footwalls of order 1 km in height (Fig. 1). GPS measurements show that the Gulf of Corinth (e.g., Fig. 1 inset) is currently extending at a rate of ~12 mm/yr at its western end, and 6 mm/yr in the east (Clarke et al., 1998; Avallone et al., 2004), and a variety of estimates of Quaternary and Holocene slip rates on the bounding faults are consistent with these rates (e.g., Armijo et al., 1996; Leeder et al., 2003; Pirazzoli et al., 2004; Bell et al., 2008). In contrast, the geomorphically similar Gulf of Evia is, according to geodetic measurements, extending at a rate of only 1–3 mm/yr; that is up to 10 times slower than the Gulf of Corinth (Clarke et al., 1998), raising the question of whether there may be a discrepancy between geodetic and geological measurements of slip rate here.

ACTIVE FAULTING IN THE LOCRIS HALF-GRABEN

The Northern Gulf of Evia is bounded to its south by three north-dipping, and segmented, fault systems (named the Coastal, Kallidromon, and Parnassos fault systems, Fig. 1) that form a series of half-graben, collectively known as the Locris half-graben. The Kamena Vourla fault, which is the principal focus of our study, is the central segment of the Coastal Fault System. Several exposures of late Quaternary fault scarps in limestone are observed along the Coastal Fault System (e.g., Jackson and McKenzie, 1999). Jackson (1999) uses the geomorphology of the region to suggest that the Coastal Fault System is both the most active, and also the youngest, of the three fault systems in the Locris half-graben.

The only recorded large earthquakes in the entire Locris region during the past ~300 yr are two earthquakes in 1894 that ruptured the

Geosphere; October 2010; v. 6; no. 5; p. 583–593; doi: 10.1130/GES00542.1; 5 figures; 2 tables.

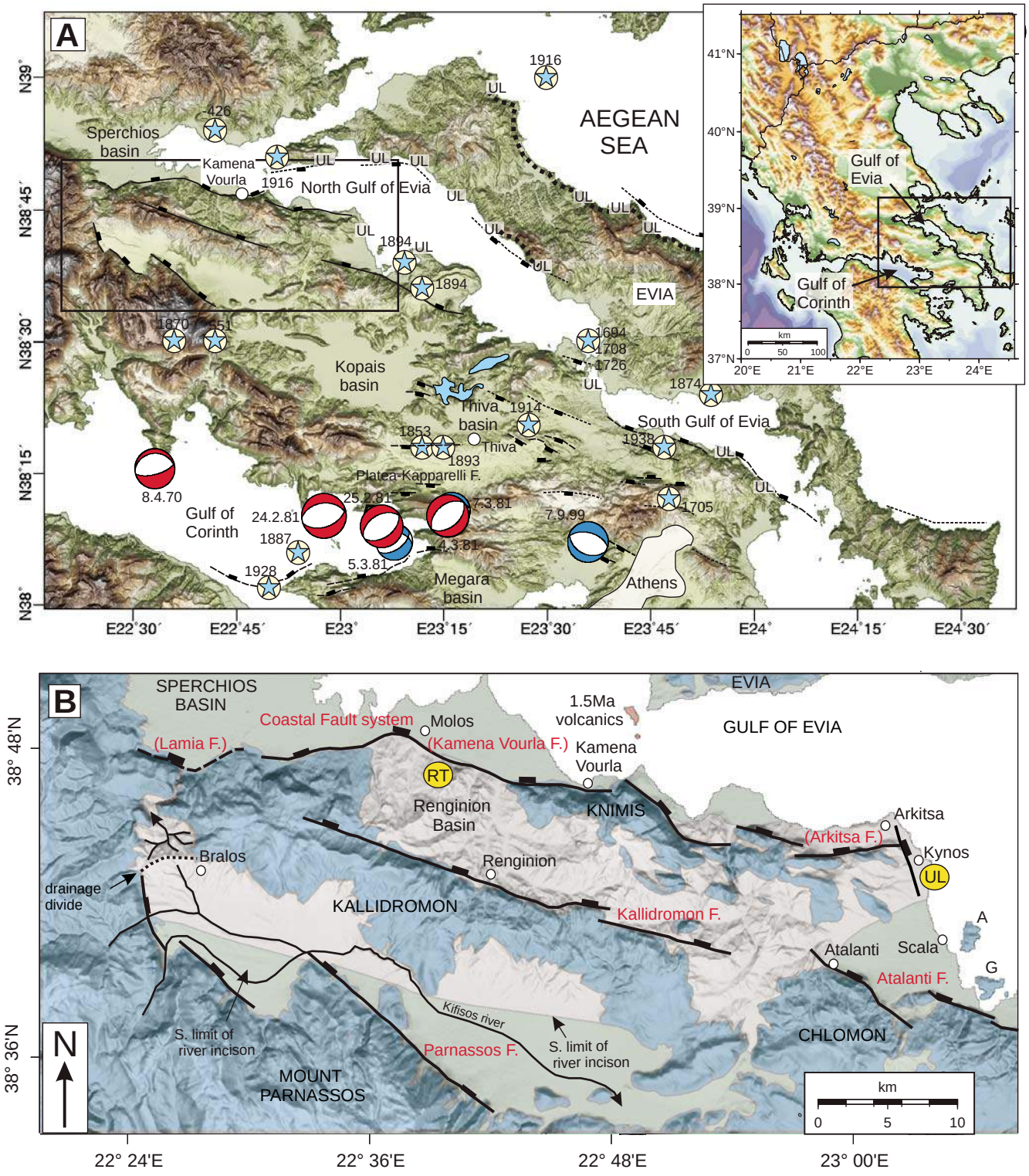

Figure 1. (A) Shaded-relief topography of the Gulf of Evia and surroundings (adapted from Goldsworthy et al., 2002). Fault-plane solutions of instrumental earthquakes are from the Harvard CMT catalog (blue) and from body-waveform modeling (red). Epicenters of historical earthquakes (represented by blue stars in white circles) are from (Goldsworthy et al., 2002, and references therein). Locations marked "UL" have lithophaga borings uplifted above sea level (Smith, 1994). Thick dotted lines mark locations of elevated shorelines (Stiros et al., 1992). (B) Geological and geomorphic map of the study area (adapted from Goldsworthy and Jackson, 2001). Regions of Mesozoic limestone bed-rock exposure are colored blue. Flat-lying sediments are green. Regions of incised sedimentary cover are marked in white. Lithophaga borings uplifted above sea level at Kynos are marked "UL." River terraces near the village of Molos are marked by "RT."

Atalanti fault (Figs. 1A and 1B; Ambraseys and Jackson, 1990; Cundy et al., 2000; Pantosti et al., 2001, 2004; Ganas et al., 2006). The larger of these two earthquakes had a magnitude of ~6.8 (Pantosti et al., 2001). The occurrence of these two earthquakes on the Atalanti fault raises the question of what is the probable earthquake repetition time of other nearby faults, including the Kamena Vourla and Lamia faults, which lie close to large towns (Fig. 1). The Atalanti lies along strike from the Kallidromon fault (Fig. 1), which lies inland from, and is subparallel to, the Coastal Fault System. Jackson (1999) argues from the geomorphology that the Kallidromon fault is less active than the Coastal Fault System, but if—as suggested by its close spatial association with the Atalanti fault—it retains some level of activity at the present day, the slip rates on the coastal system will be lower than on the Atalanti fault. It has been argued, however, that Atalandi is actually a segment of the Coastal Fault System that has stepped to the south, in which case the slip rate on the Kallidromon fault could be negligible, and the slip rate on the Kamena Vourla and Lamia faults could be comparable to that on the Atalanti fault.

SLIP RATE ON THE KAMENA VOURLA FAULT

River terraces are commonly used to calculate the late Quaternary and Holocene slip rates on fault systems because they allow measurement of the displacement of the terrace surface as well as providing material that is useful for determining the age of the surface (e.g., Lavé and Avouac, 2000). We describe two fluvial terraces of a small, unnamed, river near the village of Molos (Fig. 1B); the lower of which is displaced as it crosses the Kamena Vourla normal fault.

The Fluvial Terraces at Molos

A prominent terrace level ~20 m above the present-day bed of the river was first reported by Jackson (1999), who noted that the terrace has a similar gradient to the present-day river, and hence speculatively assigned an age of ~125 ka, based on an assumption that it formed during the last inter-glacial when sea level was similar to today. We visited Molos in September 2006 to survey the river terraces and to obtain samples for dating their depositional history. The geology of the catchment area is predominantly Mesozoic limestone, with relatively minor outcrops of mafic ophiolitic rocks and deep sea cherts. Aeolian deposits derived from the Saharan region are a widespread feature of the Quaternary deposition in Greece and constitute a source of fine-grained quartz (e.g., Goudie and Middleton, 2001). The mineralogy of the terrace fill reflects the local geology, being predominantly carbonate.

Two separate terrace levels were found. The two terraces were mapped in the field and remotely using stereo aerial photographs (Fig. 2). The terraces are paired and contain several meters of sedimentary deposits (e.g., Fig. 3). Precise heights were measured with differential GPS in profiles along several of the terrace remnants. The locations of GPS survey points are marked as red lines on Figure 2. Recorded heights (Fig. 4) clearly show the high and low levels of terrace on the southern side of the fault. The two terraces are, on average, ~20 m and ~8 m above the present-day riverbed.

The ~20 m terrace level consists of a series of steep cones originating from short tributary valleys of the main river channel. The terrace deposits consist of interbedded fluvial gravels and laterally continuous silt bodies. The deposition of these thick fans may have caused blockages of the main channel and ponding of the river resulting in deposition of the fine-grained, and occasionally laminated, layers from which radiocarbon and Optically Stimulated Luminescence (OSL) samples were taken (see later). Freshwater gastropods *Viviparidae* and *Condrinidae* were found within the high terrace fill. The sediment fans were subsequently incised during a period of river downcutting that appears to have continued, intermittently, to the present day.

A second prominent terrace, which probably represents a period of channel aggradation and lateral cutting, is preserved at a height of ~8 m above the present-day river level (Figs. 3A and 4). This lower terrace also contains freshwater gastropods (*Discidae* and *Hygromidae*) as well as rare charcoal and bone fragments. The terrace has been heavily modified by farming and construction close to where it crosses the fault (Fig. 4B). We were, therefore, unable to produce an uninterrupted GPS profile across the fault. We were, however, able to produce profiles along the low terrace on the southern, upthrown, side of the fault and along the surface of a single prominent terrace level, ~4 m above the present river level on the northern, downthrown side of the fault (Fig. 4B). A westward-flowing tributary stream has cut a small channel into the surface of the low terrace on the upthrown side of the fault (Fig. 4B, also see Fig. 3G). The two terrace fragments have similar gradients but are offset, vertically, by 6.0 ± 0.1 m. The terrace on the downthrown side of the fault forms the surface of a delta (Fig. 1B). It therefore appears, if our correlation of the terrace fragments to the north and south of the fault is correct, that the lower river terrace of the Molos River corresponds to a period of delta progradation into the Gulf of Evia.

The gradient of the present river is controlled by numerous small concrete dams that prevented us from obtaining a complete riverbed profile. The dams have also caused sediment to aggrade behind them, causing the river profile to consist of a series of short low-gradient sections separated by downward steps of several meters at each obstruction. One of the dams is sited close to the fault location and lowers the riverbed by several meters (Fig. 4B). The riverbed is ~4 m below the terrace surface on the downthrown, northern, side of the fault. The original river gradient is approximated by drawing a straight line between the two short surveyed parts of the riverbed. This assumed river profile is similar in gradient to those measured for the preserved terrace remnants (Fig. 4).

Dating the Fluvial Terraces

Samples were collected for both OSL and radiocarbon dating. We sampled the lower Molos terrace at two sites (Fig. 2B). Site 1 (38°47′15″N 22°41′01″E) is located immediately south of the Kamena Vourla fault and exposes ~2.5 m of laminated silts with occasional, isolated, small pebbles (Fig. 3B). The laminated silts are overlain by ~1 m of coarse fluvial gravels. The contact between silts and gravels is erosive in places, but shows interbedding in others, and indicates that there is no unconformity between the two units. Sediments below the sampled horizons contain calcretes. Two OSL samples were collected from the exposure (A at ~1.7 m below the surface and B at ~1.2 m).

A second sampling site (Sample Site 2; 38°46′28″N 22°40′51″E) is situated ~2 km south of the fault. At this site, an exposure of the lower terrace fill was found, which consisted of ~3 m of interbedded fluvial gravels and silts (Figs. 3C and 3D). Two OSL samples, along with gastropod shells (*Discidae*) and a fragment of charcoal, were taken from ~1.2 to 1.3 m below the lower terrace surface in a 1-m-thick silt and sand deposit.

The high terrace was sampled at one site (Sample Site 3, 38°46′35″N 22°40′51″E) where a thick (~1 m), laterally continuous, silt layer was exposed 4 m beneath the surface of the terrace (Figs. 3E and 3F). Three OSL samples were collected from the same layer across a depth range of ~50 cm. Gastropod shells were also collected from the silt layer (*Viviparidae viviparus, Condrinidae*).

OSL and Radiocarbon Dating Methods

Samples for optical dating were collected in opaque plastic tubing and stored in light-tight

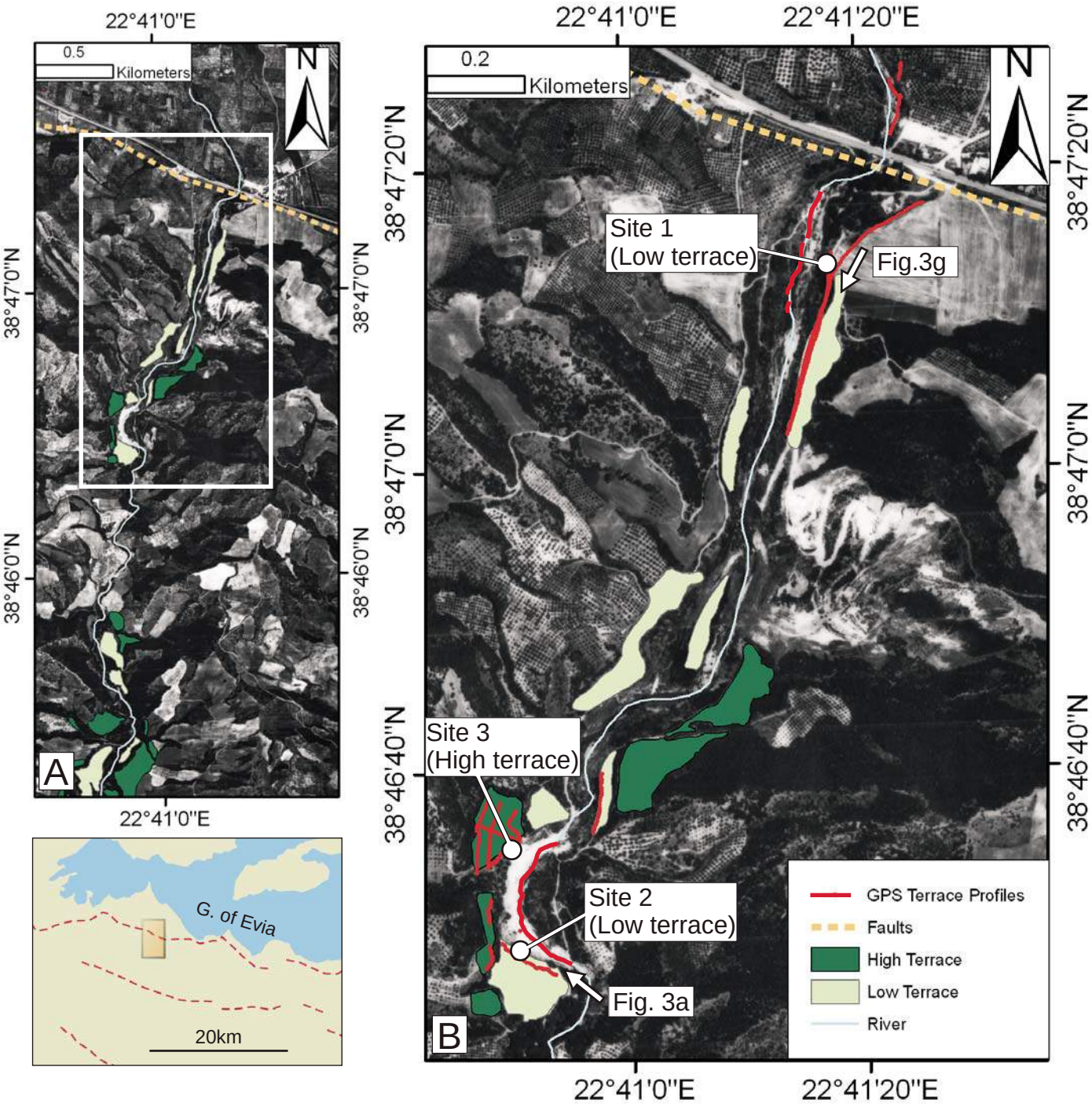

Figure 2. (A) An aerial photograph of the Renginion Basin just south of Molos. Two levels of terraces have been identified from stereo-pairs. A high terrace is marked in dark green. Remnants of a low terrace, ~8 m above the present river bed, are marked in light green. The approximate location of the Kamena Vourla fault is marked by a yellow dashed line. (B) An enlarged view of the study area. The locations of GPS profiles are shown as red lines. The three sampling sites (two from the lower terrace and one from the higher terrace) are labeled. The two white arrows show the locations, and look directions, of the photographs in Figures 3A and 3G.

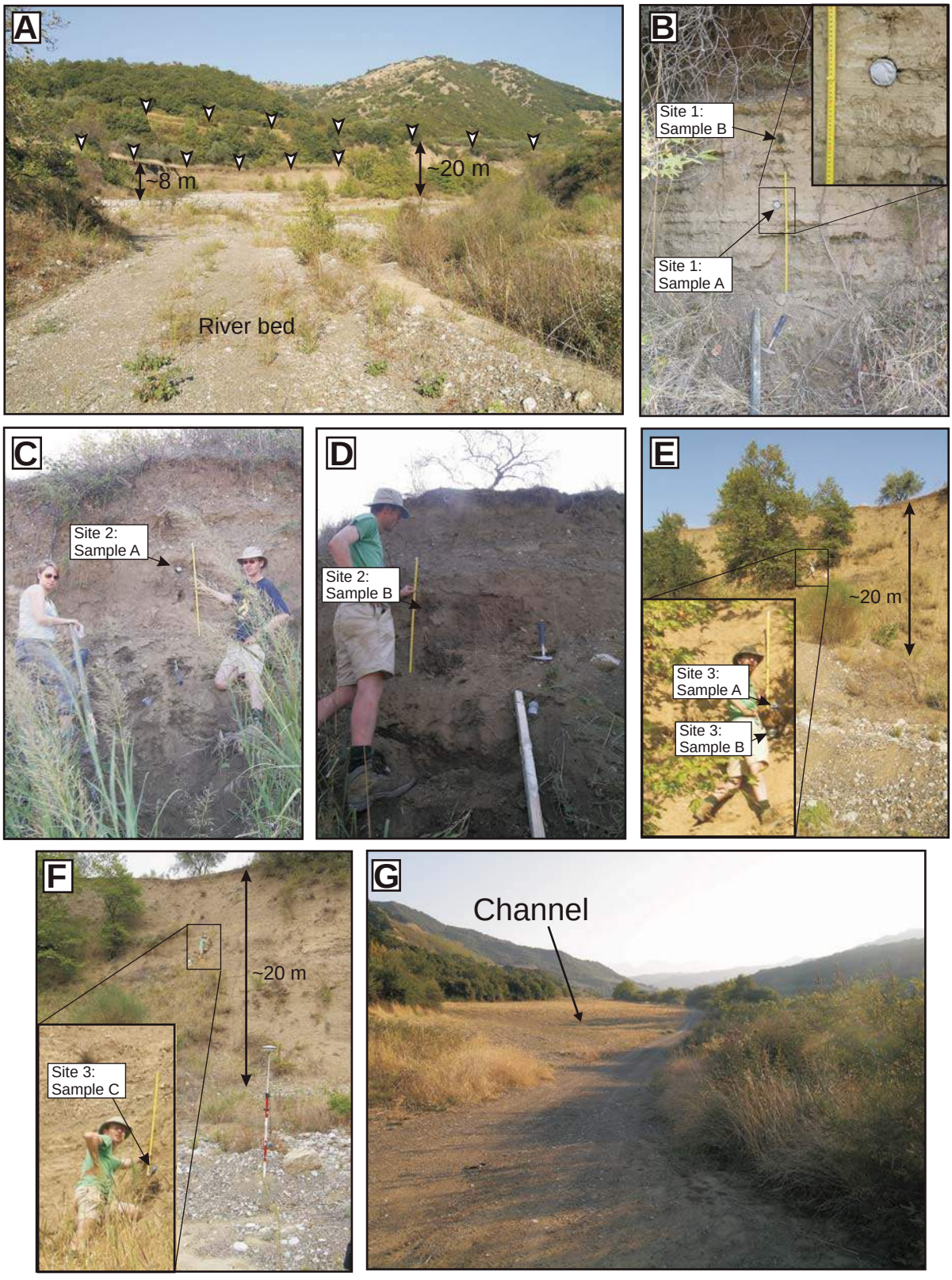

Figure 3. Field photographs of the river terraces near Molos and sampling sites. (A) View downstream showing both river terrace levels (see Fig. 2B for location). Both terrace tops are marked by vertical white arrows. (B) View east at the laminated silts exposed at Sample Site 1. The positions of the two OSL samples are marked. A 1 m scale is visible (as in all later photographs). (C-D) Sample Site 2: low terrace. Location of the two OSL samples within the deposit. (E-F) Sample Site 3: high terrace. Locations of the three OSL samples within the terrace deposits. (G) View southwards along the low terrace surface (immediately above Sample Site 1, see Fig. 2B for location). A small westward-flowing channel has cut into the otherwise planar surface in the foreground. This channel is visible on the GPS profiles in Figure 4.

bags until processed. We took care to minimize exposure of the sediment to light during sampling. The chosen surface in the terrace wall was prepared by removing the outer surface and then a plastic tube was hammered into the cleaned surface until completely full. Duct tape was used to seal the ends, protecting the sample from light exposure and moisture loss. Finally the sample was wrapped tightly in several layers of opaque black plastic. At least two samples were obtained from each of three locations. All sample locations are shown in Figure 3.

Sample preparation was conducted at the Oxford Luminescence Dating (OLD) laboratory under subdued red light. The first 3 cm of sediment from the top and bottom of the plastic sample tubes were removed due to potential light exposure, and used to determine moisture content by weighing, drying at 40 °C in the laboratory, and reweighing. The remaining shielded sediment from the center of the tube was then used for equivalent dose (De) determination. In view of the silt-rich nature of the sediment, the 4–11 µm ("fine-grain") fraction was isolated for analysis by settling according to Stokes' law. The sample was treated with excess 35% hydrochloric acid until no further reaction was observed to remove the high concentration of carbonate, and then 37% hydrogen peroxide in order to remove organic matter. To remove feldspars, the samples were finally treated in 35% fluorosilicic acid for two weeks; the long treatment time was selected to ensure that the dissolution of feldspars was complete. The fine-grained samples, assumed to be composed of isolated quartz, were then mounted on aluminum disks by evaporation from an acetone suspension.

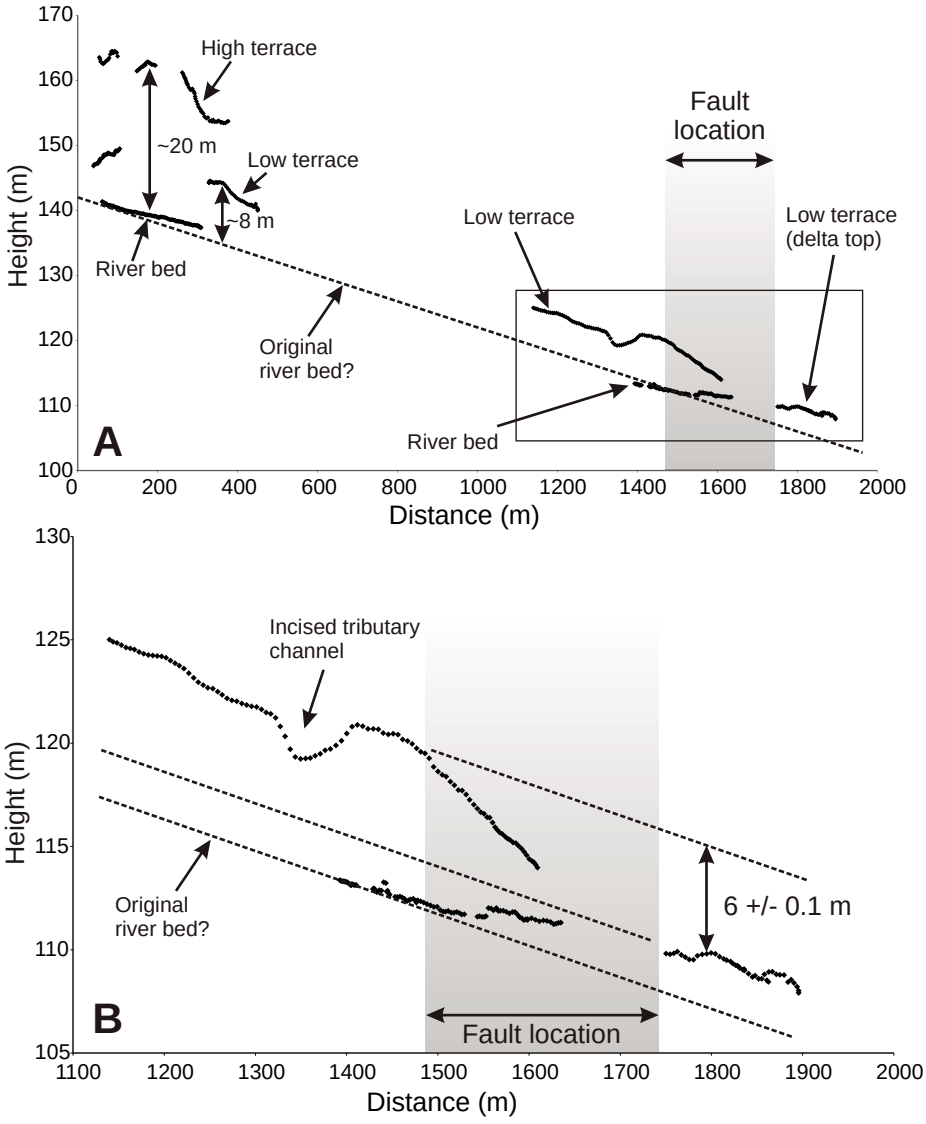

Figure 4. (A) Kinematic GPS profiles along the surfaces of the upper and lower terraces and the river bed. The GPS data is projected onto a single profile line running along the direction of the river and perpendicular to the fault. The Kamena Vourla fault is located somewhere within the gray region (1500–1750 m along the profile). As the present-day river bed has been modified, we approximate the original river gradient by a dotted line. (B) A close up view of the lower terrace surface where it crosses the fault. There is a 6 ± 0.1 m vertical displacement of the terrace surface as it crosses the fault.

Measurements were conducted on a Riso TL/OSL-DA-15 system (Botter-Jensen et al., 2000). Initial tests (Duller, 2003) suggested a persistent feldspar contamination, which, albeit much reduced, was still present following a further two weeks in fluorosilicic acid. Samples were thus analyzed using a post-IR blue OSL procedure (Banerjee et al., 2001) within the single-aliquot regenerative (SAR) protocol (Murray and Wintle, 2000) to minimize any malign effects of feldspar luminescence. The resultant luminescence signals were relatively dim yet generally yielded usable growth curves; the few aliquots that failed recycling or recuperation tests were rejected. Approximately ten disks were analyzed from each sample, and dose distributions from these are shown in Figure 5.

The environmental dose rate was determined from ICP-MS/AES (inductively coupled plasma mass spectrometry/atomic emission spectrometry) of K, U, and Th concentrations at Royal Holloway University of London. Radioisotope concentrations were converted to dose rate using the conversion factors of Adamiec and Aitken (1998) and grain-size attenuation factors of Mejdahl (1979). Cosmic dose rates, including variations due to depth of burial, altitude, and geomagnetic latitude, were calculated using the equation of Prescott and Hutton (1994). Attenuation of radioactivity dose by interstitial water was corrected for using the absorption coefficient of Zimmerman (1971). Estimating the long-term water content of the sediment is a significant source of error in luminescence age determinations because of possible variations in pore water content since burial. It was assumed that present-day moisture content was representative of water contents throughout burial (percentage dry weight of sample) with a 5% error to reflect uncertainty in estimation. The ages calculated from these measurements are shown in Table 1.

Both the upper and lower terraces contained gastropods typical of freshwater faunas of the region (Kerney and Cameron, 1979; Davies, 1971). To compliment the OSL dates, we

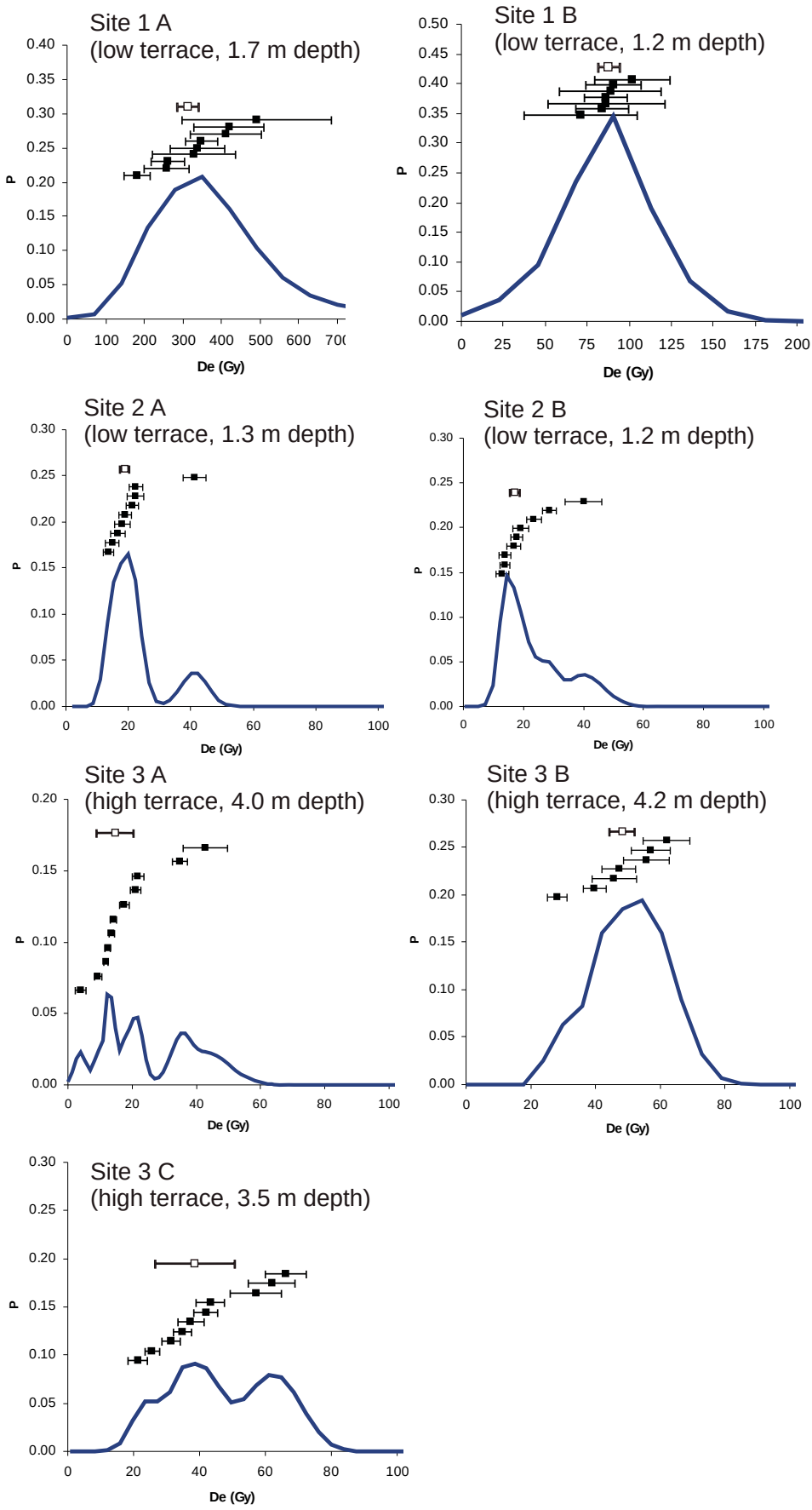

Figure 5. Probability density plots of the equivalent dose from single-aliquot regenerative (SAR) OSL for each of the fluvial terrace samples listed in Table 1. Standard error is reported for all samples except 3A and 3C, which show complex multimodal and overdispersed dose distributions, possibly suggestive of poor bleaching or postdepositional sediment disturbance. For samples 3A and 3C, the weighted mean and the standard deviation provide a reasonable estimate of the major peak in each case, albeit at the expense of very large uncertainties on the dose estimate.

Table 1. OSL DATES FOR THE FLUVIAL TERRACE SAMPLES AT MOLOS

Lab ID	Sample ID	Depth (m)	K (%)	Th (ppm)	U (ppm)	Cosmic dose rate (Gy/ka)	Moisture (%)	Dose rate (Gy/ka)	Equivalent dose (Gy)	Age (ka)
OxL-1719	Site 1 A (low terrace)	1.7	1.070±0.054	5.250±0.263	1.290±0.065	0.160±0.013	0.01±0.05	2.228±0.170	313.6±28.5	140.7±16.8
OxL-1720	Site 1 B (low terrace)	1.2	1.080±0.054	4.940±0.247	1.300±0.065	0.173±0.014	0.01±0.05	2.224±0.170	87.8±6.3	39.5±4.1
OxL-1717	Site 2 A (low terrace)	1.3	1.260±0.063	5.540±0.277	1.270±0.064	0.172±0.014	0.03±0.05	2.397±0.180	18.2±1.6	7.6±0.9
OxL-1718	Site 2 B (low terrace)	1.2	1.180±0.059	4.880±0.244	1.200±0.060	0.174±0.014	0.03±0.05	2.232±0.170	17.0±1.9	7.6±1.0
OxL-1714	Site 3 A (high terrace)	4.0	1.040±0.052	4.160±0.208	1.040±0.052	0.115±0.010	0.01±0.05	1.945±0.150	38.9±4.6	20.0±2.8
OxL-1715	Site 3 B (high terrace)	4.2	1.200±0.060	5.230±0.262	1.260±0.063	0.112±0.010	0.04±0.05	2.217±0.170	48.0±3.8	21.6±2.4
OxL-1716	Site 3 C (high terrace)	3.5	1.130±0.057	5.250±0.263	1.200±0.060	0.123±0.011	0.02±0.05	2.194±0.170	38.7±12.2	17.6±5.7

Note: Samples were collected from three sites (Figs. 2 and 3; locations are given in section Dating the Fluvial Terraces). Details of the procedures for calculating dose rates are given in the text (section OSL and Radiocarbon Dating Methods).

TABLE 2. RADIOCARBON DATES FOR THE RIVER TERRACE SAMPLES AT MOLOS AND LITHOPHAGA SHELLS FROM KYNOS

Publication code	Sample Identifier	Material	^{14}C enrichment (% modern ± 1 sigma)	Conventional radiocarbon age (years BP ± 1 sigma)	Carbon content (% by wt.)	$\partial^{13}C_{VPDB}$‰	Calibrated age (± 2 sigma)
SUERC-13102	Site 2	Charcoal	94.12 ± 0.41	487±35	50.9	-26.1	1397–1457 A.D.
SUERC-13104	Site 3	*Viviparidae*	65.13±0.28	3445±35	11.8	-7.9	1882–1681 B.C.
SUERC-13107	Site 2	*Discidae*	78.49±0.34	1945±35	12.2	-9.2	3 B.C.–128 A.D.
SUERC-13108	L9	*Lithophaga*	61.51±0.27	3903±35	10.1	2.7	1821–1662 B.C.
SUERC-13109	L10	*Lithophaga*	60.90±0.27	3984±35	11.0	1.8	1910–1758 B.C.

Note: Conversion of ^{14}C ages into calibrated dates was performed using the program of Stuiver and Reimer (1993) and with calibration data from Reimer et al. (2004).

selected a single gastropod shell from each of the 20 m and 8 m terrace levels, as well as a small charcoal fragment found in the 8 m terrace, for radiocarbon analysis. The raw samples were cleaned and photographed for identification before undergoing further pretreatments at the NERC Radiocarbon Laboratory to prepare the samples to graphite. ^{14}C concentrations were then measured at the SUERC (Scottish Universities Environmental Research Centre) AMS Facility (5 MV, National Electostatic Corporation). Results are reported as conventional radiocarbon yr B.P. (relative to AD 1950) and % modern ^{14}C, both expressed at the ±1 sigma level for overall analytical confidence (Table 2). The ^{14}C ages (yr B.P. ± 1 sigma) were converted into calibrated dates using the program of Stuiver and Reimer (1993) (http://www.calib.org/) and with calibration data from Reimer et al. (2004).

Summary of Terrace Age Data

Comparison of the data in Tables 1 and 2 highlights considerable variation in the available age constraints, both among ^{14}C and OSL dates from the same locations, and between separate sampling sites. The large amount of variability in the age data precludes any firm conclusions being drawn from them on the age of the terraces. At Sampling Site 1, close to the Kamena Vourla fault (Fig. 2B), OSL samples were obtained from depths of 1.7 m and 1.2 m within a single laminated silt body (Fig. 3B) that yielded ages 100 ka apart (~40 and 140 ka, Table 1). Although the two ages are in the correct stratigraphic order, it is unlikely that both ages represent real deposition ages at this site, because this would imply only ~60 cm of deposition over a period of 100 ka.

At Sampling Site 2 (Figs. 3C and 3D) we collected two OSL samples from the lower terrace. These samples, which were taken from approximately the same level within the deposits, yielded consistent ages of 7.6 ± 0.9 ka and 7.6 ± 1.0 ka (Table 1). Two ^{14}C ages, also from the same stratigraphic level, yielded ages of ~2 ka (3 B.C. to 128 A.D.) from analysis of a *Discidae* gastropod shell and ~0.5 ka (1397–1457 A.D.) from a charcoal fragment (Table 2). There is a clear mismatch between the OSL and ^{14}C ages. There is also somewhat of a mismatch between the two radiocarbon ages, although both place the deposition within the historical period.

A similar mismatch between OSL and ^{14}C ages is found for the upper terrace level (at Site 3, Tables 1 and 2). Three OSL ages are consistent with one another (20.0 ± 2.8 ka, 21.6 ± 2.4 ka, and 17.6 ± 5.7 ka). The single ^{14}C age, obtained from a *viviparidae Viviparus* gastropod shell, provides a much younger age of ~3.5 ka (1397–1457 B.C.; Table 2).

The implausible ages of 40 and 140 ka from two adjacent samples of the lower terrace at Site 1 preclude any firm conclusions being drawn from any of the OSL data. Although we have two near identical OSL ages of ~7.6 ka for the lower terrace at Site 2, and three samples from the higher terrace at Site 3 that show ages of ~20 ka, each of these could also be misleading and should be treated with caution. However, as we shall see in the section Palaeoenvironmental Constraints on Terrace Age, there are independent reasons from the palaeo-environmental record for the OSL age of ~7.6 ka to be roughly indicative of the deposition age of the lower terrace.

In all cases, the ^{14}C ages are younger, by a large factor, than the OSL ages for the equivalent sites. The ^{14}C ages should, however, also be treated with a high degree of caution due to the very small sample set and the discrepancies in age within this set (Table 2). The depositional environment of the river terraces is rich in carbonate and the gastropod shells may have formed out of equilibrium with atmospheric ^{14}C (e.g., Goodfriend and Stipp, 1983; Goodfriend and Hood, 1983). It is unclear, however, why the dates would be skewed toward younger, rather than older, apparent ages. The discrepancy may in fact be due to the gastropod shells and charcoal used for ^{14}C dating having become incorporated into the terrace fill after deposition such that they provide anomalously young ages. With the small number of radiocarbon dates available it is difficult to fully assess the reliability of the ages.

Palaeoenvironmental Constraints on Terrace Age

The available quantitative age data are too scattered to be of use in forming conclusions on the deposition age of the two river terraces. However, the location and distribution of the lower terrace hold clues to its likely age.

Prior to stabilizing at its present-day level at ~6 ka, the water level in the Gulf of Evia was several tens of meters lower than today, and the river systems draining into it would thus grade to a lower baselevel. We would, therefore, not expect fluvial terraces formed prior to 6 ka to be preserved, as they would now have been buried due to aggradation in the river system as sea level rose. The lower terrace extends northwards to the Kamena Vourla fault, it is therefore not a localized feature formed in response to a blockage within the river catchment, and it is highly probable that it connected with the delta surface—which has the same gradient though it is now displaced vertically by 6 m—in the immediate hanging-wall of the fault. The surface of the delta reflects stabilization of the sea surface at its present-day maximum and subsequent northwards progradation of the delta into the Gulf of Evia. The lower terrace is then likely to represent aggradation within the river catchment synchronous to progradation of the delta at ~6 ka. This argument, based on the changes in sea level during and after the last glacial period and the likely consequences these changes would have on the hydrology of rivers draining into the Gulf, is the most probable scenario given the absence of robust dating results.

The two near identical OSL ages of ~7.5 ka at Site 2 are consistent with the above scenario and, although caution should be applied in interpretation of the dating results, may be indicative of the real deposition age of the lower terrace. Continuing with this reasoning, if the three similar OSL ages of ~20 ka from the upper terrace at Site 3 also represent the real deposition age, it suggests that the upper terrace formation—which is more accurately a series of small alluvial fans originating from small tributaries—occurred at or near the last glacial maximum. At this time, a minimum is recorded in the arboreal/nonarboreal pollen ratio from three separate lake cores in Greece, which is interpreted as reflecting a collapse in the population of temperate trees (e.g., Tzedakis et al., 2004). In turn, this change in vegetation could have destabilized hill slopes, leading to increased sediment supply to the Molos river channel. The rapid recovery of the temperate forest during the last deglaciation (e.g., Okuda et al., 2001) could have terminated this period of aggradation.

We note, however, that a sequence of fan deposition, incision, and delta progradation all taking place during the last ~3.5 ka, as suggested by the scarce radiocarbon data, is also quite possible. For instance, the Sperchios delta (Fig. 1) has prograded ~10 km into the northern Gulf of Evia since 480 B.C. (Kraft et al., 1987; Eliet and Gawthorpe, 1995) showing that relatively large amounts of sedimentation could have occurred over rather short time scales. We cannot, however, tie the radiocarbon ages to particular climatic events in the past 3.5 ka.

Estimate of the Rates of Slip and Extension across the Kamena Vourla Fault

We correlate the lower river terrace (on the southern, upthrown, side of the fault) with the surface of a delta on the northern, downthrown, side of the fault (see section The Fluvial Terraces at Molos). In the absence of definitive age constraints on the lower terrace we assume that it formed at ~6 ka when sea level stabilized at its present-day maximum (see section Dating the Fluvial Terraces). The terrace is offset

vertically by 6 m across the fault (Fig. 4); the vertical component of displacement across the Kamena Vourla fault is therefore estimated to be ~1 mm/yr.

We now compare our estimate of vertical displacement rate with the extension rates measured by GPS across the Locris half-graben and the Gulf of Evia; those rates are not well resolved, but are probably no higher than 1–3 mm/yr (Clarke et al., 1998). We place bounds on the horizontal extension across the fault by assuming a fault dip of 30°–60°, which is the typical range observed for seismogenic normal faults (Jackson and White, 1989). A dip range of 30°–60° gives a rate of extension across the fault of 0.6–1.7 mm/yr. The estimated rate of extension across the Kamena Vourla fault lies within the range of extension rates (1–3 mm/yr) for the region surrounding the northern Gulf of Evia measured by GPS.

SLIP RATE ON THE ATALANTI AND ARKITSA FAULT SEGMENTS

We now discuss our estimate of the slip rate for the Kamena Vourla fault in the wider setting of the northern Gulf of Evia. The Kamena Vourla fault continues eastwards for ~30 km, where it terminates at the western end of the Arkitsa fault (Fig. 1B). The next major fault to the east is the Atalanti fault, beginning at a longitude of ~23°E (Fig. 1B), and 10 km to the south of the Arkitsa fault.

The Late Cenozoic slip rate of the Atalanti fault was estimated at 0.1–0.5 mm/yr by Pantosti et al. (2001) based on an assumed 130–35 ka age of a terrace displaced vertically by 10–19 m across the fault. Palaeoseismic trenching across the Atalanti fault (Pantosti et al., 2004), with age control provided by radiocarbon and archaeological dating, suggests a repeat time of 660–1120 yr between earthquakes, with evidence for three events: one between 50 B.C. and A.D. 230, a second between A.D. 770 and 1160, and the historical 1894 earthquakes. The results from palaeoseismology indicate an average slip rate of 0.4–1.6 mm/yr on the fault: consistent with its accommodating a large proportion of the 1–3 mm/yr of present-day extension across the region. The Atalanti fault is, therefore, usually considered to be an eastward continuation of the coastal fault system that has stepped southwards from the Arkitsa segment (e.g., Pantosti et al., 2001; Goldsworthy and Jackson, 2001; Fig. 1b). These estimates of slip rate on the Atalanti fault are consistent with our assumed estimate of ~1–2 mm/yr for the Kamena Vourla fault, and suggest that the Atalanti fault forms part of the most active, frontal, faults of the region, despite lying directly along strike from the Kallidromon fault, which is known to be slipping much less rapidly than the frontal faults (e.g., Jackson, 1999).

The only other quantitative estimate of slip rate of the Coastal Fault System comes from the eastern end of the Arkitsa segment near the village of Kynos (Fig. 1B), where there are abundant indications of coastal uplift including a coastal notch at ~1.4 m above present sea level (Pirazzoli et al., 1999), marine terraces, and raised beaches (Dewez, 2003; Goldsworthy and Jackson, 2001). Radiocarbon dating of *Lithophaga* shells preserved below the ~1.4 m coastal notch at Kynos by Pirazzoli et al. (1999) yielded ages that were a maximum of ~2.7–3.4 ka (800–1410 B.C.) at 0.5 m above sea level and which decreased upwards, to ~1.7–2.3 ka (210 A.D.–360 B.C) at 1.4 m elevation. Two new radiocarbon ages (presented in Table 2), for *Lithophaga* shells from ~1.2 m above sea level, yield calibrated ages of ~3.6–3.7 ka (1662–1821 B.C.) and 2.1–3.7 ka (190–1758 B.C.) These ages are older than, but are from a level between, the elevations sampled by Pirazzoli et al. (1999).

The notch at ~1.4 m is likely to represent, as has been measured in several other parts of Greece (e.g., Pirazzoli et al., 2004), uplift of the coast relative to sea level since it stabilized at ~6 ka. The *Lithophaga* extracted from levels below the notch represent emergence of these levels and the ages are hence younger than 6 ka. Using the assumption of a 6 ka age for the coastal notch, Goldsworthy and Jackson (2001) obtained an estimate of ~0.2 mm/yr for the rate of uplift relative to sea level at Kynos. The range of uplift rates can be converted into rates of total vertical displacement by assuming a long-term uplift-to-subsidence ratio of between 1:2 and 1:4 (e.g., Stein and Barrientos, 1985). Goldsworthy and Jackson's (2001) estimate translates to a slip rate of 0.7–1.2 mm/yr for a fault dipping at 60°, as measured from exposures of the Arkitsa fault plane (Jackson and McKenzie, 1999), or 1.2–2.0 mm/yr if the fault dips at 30°.

Interpretation of the uplift rate at Kynos in terms of a slip rate on the Arkitsa fault is complicated by the location of the site at the eastern tip of the fault segment: whether a slip-rate estimate from the tip of a fault segment is likely to be representative of the average rate of slip along the length of that segment is debatable, and the Holocene slip rate on the Arkitsa fault segment is far from resolved. But given that the uplifted coastal notches at Kynos are likely to date from a maximum of ~6 ka, a tentative minimum estimate of slip rate of 0.7–2.0 mm/yr can be estimated, at this one site, for a fault dip in the range 30°–60°.

DICUSSION AND CONCLUSIONS

Displacement of the lower of the two river terraces described in the section Slip Rate on the Kamena Vourla Fault, combined with an assumption that the terrace dates from ~6 ka, indicates that the Kamena Vourla normal fault slips at a rate of ~1.2–2.0 mm/yr and accommodates ~0.6–1.7 mm/yr of extension. An estimate of slip rate on the Atalanti fault segment suggests a similar slip rate of 0.4–1.6 mm/yr (Pantosti et al., 2004). The slip rate of the Arkitsa fault is the least well-constrained of the three segments, and is complicated by the location of the only study site at the tip of the fault segment, but if the uplifted coastal notches at Kynos are assumed to have formed at ~6 ka the corresponding slip rate is 0.7–2.0 mm/yr.

The simplest interpretation of these data is that the Kamena Vourla, Arkitsa, and Atalanti faults are the dominant active faults on the south coast of the northern Gulf of Evia, and that they are all slipping at a similar rate of ~1–2 mm/yr. We are not aware of any estimates of slip rate on the Lamia fault, to the west of Kamena Vourla and close to the conurbation of Lamia (Fig. 1), but as it forms the western segment of the Coastal Fault System, and is morphologically similar to the eastern segments, we might expect a similar slip rate on that fault as well.

The range of slip-rate estimates is at the lower end, though of the same order, as the 1–3 mm/yr of present-day extension suggested by GPS and suggests that the Gulf of Evia region is not subject to large temporal variations in extension rate over Holocene time scales. However, our study shows the need for an improved geodetic estimate of the extension rate across this region. The total extension rate at the present day is ~1–3 mm/yr. If the true figure is only ~1 mm/yr, then it seems likely that the segments of the Coastal Fault System are the major active faults of the region. If, however, the geodetic rate is closer to 3 mm/yr, it suggests that other faults in the Gulf of Evia region, in particular those that are inferred to bound the northern coast of the Gulf (Fig. 1), pose a comparable hazard.

ACKNOWLEDGMENTS

Isabelle Ryder, Mike Floyd, John Elliot, Juliet Biggs, and Ivana Barisin helped in various aspects of the preparation of this paper. We thank Demitris Paradissis for obtaining the satellite photographs and the Department of Earth Sciences at Oxford University for partially covering field costs. We are grateful to James Jackson and an anonymous reviewer for detailed and helpful review comments that greatly improved the manuscript. R.T.W. is supported by a Royal Society University Research Fellowship though the fieldwork was performed while he was supported by a NERC Post-doctoral Fellowship.

REFERENCES CITED

Adamiec, G., and Aitken, M., 1998, Dose rate conversion factors: Update: Ancient Thermoluminescence, v. 16, p. 37–49.

Ambraseys, N., and Jackson, J., 1990, Seismicity and associated strain of central Greece between 1890 and 1988: Geophysical Journal International, v. 101, p. 663–708, doi: 10.1111/j.1365-246X.1990.tb05577.x.

Armijo, R., Meyer, B., King, G., Rigo, A., and Papanastassiou, D., 1996, Quaternary evolution of the Corinth rift and its implications for the late Cenozoic evolution of the Aegean: Geophysical Journal International, v. 126, p. 11–53, doi: 10.1111/j.1365-246X.1996.tb05264.x.

Avallone, A., Briole, P., Agatza-Balodimou, A.M., Biliris, H., Charade, O., Mitsakaki, C., Nercessian, A., Papazissi, K., Paradissis, D., and Veis, G., 2004, Analysis of eleven years of deformation measured by GPS in the Corinth Rift Laboratory area: Comptes Rendus Geosciences, v. 336, p. 301–311.

Banerjee, D., Murray, A.S., Botter-Jensen, L., and Lang, A., 2001, Equivalent dose estimation from a single aliquot of polymineral Fine-grains: Radiation Measurements, v. 33, p. 73–93, doi: 10.1016/S1350-4487(00)00101-3.

Bell, R., McNeill, L., Bull, J., and Henstock, T., 2008, Evolution of the offshore western Gulf of Corinth: Geological Society of America Bulletin, v. 120, p. 156–178, doi: 10.1130/B26212.1.

Botter-Jensen, L.B.E., Duller, G.A.T., and Murray, A.S., 2000, Advances in luminescence instrument systems: Radiation Measurements, v. 32, p. 523–528, doi: 10.1016/S1350-4487(00)00039-1.

Clarke, P.J., Davies, R.R., England, P.C., Parsons, B.E., Billiris, H., Paradissis, D., Veis, G., Cross, P.A., Denys, P.H., Ashkenazi, V., Bingley, R., Kahle, H.G., Muller, M.V., and Briole, R., 1998, Crustal strain in central Greece from repeated GPS measurements in the interval 1989–1997: Geophysical Journal International, v. 135, p. 195–214, doi: 10.1046/j.1365-246X.1998.00633.x.

Cundy, A., Kortekaas, S., Dewez, T., Stewart, I., Collins, P., Croudace, I., Maroukian, H., Papanastassiou, D., Gaki-Papanastassiou, P., Pavlopoulos, K., and Dawson, A., 2000, Coastal wetlands as recorders of earthquake subsidence in the Aegean: A case study of the 1894 Gulf of Atalanti earthquakes, central Greece: Marine Geology, v. 170, p. 3–26, doi: 10.1016/S0025-3227(00)00062-1.

Davies, M., 1971, Tertiary faunas: A text-book for oil palaeontologists and students of geology: London, George Allen and Unwin, v. 1.

Dewez, T., 2003, Geomorphic markers and digital elevation models as tools for tectonic geomorphology in central Greece [Ph.D. thesis]: Uxbridge, Brunel University.

Duller, G.A.T., 2003, Distinguishing quartz and feldspar in single grain luminescence measurements: Radiation Measurements, v. 37, no. 2, p. 161–165, doi: 10.1016/S1350-4487(02)00170-1.

Eliet, P.P., and Gawthorpe, R.L., 1995, Drainage development and sediment supply within rifts, examples from the Sperchios basin, central Greece: Journal of the Geological Society, v. 152, p. 883–893, doi: 10.1144/gsjgs.152.5.0883.

Ganas, A., Sokos, E., Agalos, A., Leontakianakos, G., and Pavlides, S., 2006, Coulomb stress triggering of earthquakes along the Atalanti Fault, central Greece: Two April 1894 M6+ events and stress change patterns: Tectonophysics, v. 420, p. 357–369, doi: 10.1016/j.tecto.2006.03.028.

Goldsworthy, M., and Jackson, J., 2000, Active normal fault evolution in Greece revealed by geomorphology and drainage patterns: Journal of the Geological Society, v. 157, p. 967–981, doi: 10.1144/jgs.157.5.967.

Goldsworthy, M., and Jackson, J., 2001, Migration of activity within normal fault systems: Examples from the Quaternary of mainland Greece: Journal of Structural Geology, v. 23, p. 489–506, doi: 10.1016/S0191-8141(00)00121-8.

Goldsworthy, M., Jackson, J., and Haines, A.J., 2002, The continuity of active fault systems in Greece: Geophysical Journal International, v. 148, p. 596–618, doi: 10.1046/j.1365-246X.2002.01609.x.

Goodfriend, G.A., and Hood, D.G., 1983, Carbon isotope analysis of land snail shells: Implications for carbon sources and radiocarbon dating: Radiocarbon, v. 25, p. 810–830.

Goodfriend, G.A., and Stipp, J.J., 1983, Limestone and the problem of radiocarbon dating of land-snail shell carbonate: Geology, v. 11, p. 575–577, doi: 10.1130/0091-7613(1983)11<575:LATPOR>2.0.CO;2.

Goudie, A.S., and Middleton, N.J., 2001, Saharan dust storms: Nature and consequences: Earth-Science Reviews, v. 56, p. 179–204, doi: 10.1016/S0012-8252(01)00067-8.

Jackson, J., 1994, Active tectonics of the Aegean region: Annual Review of Earth and Planetary Sciences, v. 22, p. 239–271, doi: 10.1146/annurev.ea.22.050194.001323.

Jackson, J., 1999, Fault death: A perspective from actively deforming regions: Journal of Structural Geology, v. 21, p. 1003–1010, doi: 10.1016/S0191-8141(99)00013-9.

Jackson, J., and McKenzie, D., 1999, A hectare of fresh striations on the Arkitsa fault, central Greece: Journal of Structural Geology, v. 21, p. 1–6, doi: 10.1016/S0191-8141(98)00091-1.

Jackson, J., and White, N.J., 1989, Normal faulting in the upper continental crust; observations from regions of active extension: Journal of Structural Geology, v. 11, p. 15–36, doi: 10.1016/0191-8141(89)90033-3.

Kerney, M.P., and Cameron, R.A.D., 1979, A Field Guide to the Land Snails of Britain and North-west Europe: London, Collins.

Kraft, J.C., Rapp, G., Szemler, G.J., Tziavos, C., and Kase, E.W., 1987, The pass at Thermopylae, Greece: Journal of Field Archaeology, v. 14, p. 181–198, doi: 10.2307/530139.

Lavé, J., and Avouac, J.P., 2000, Active folding of the fluvial terraces across the Siwalik Hills, Himalayas of Central Nepal: Journal of Geophysical Research, v. 105, B3, p. 5735–5770, doi: 10.1029/1999JB900292.

Leeder, M., McNeill, L., Collier, R., Portman, C., Rowe, P., Andrews, J., and Gawthorpe, R., 2003, Corinth rift margin uplift: New evidence from late Quaternary marine shorelines: Geophysical Research Letters, v. 30, p. 1611–1614, doi: 10.1029/2003GL017382.

Mejdahl, V., 1979, Thermoluminescence dating: Beta-dose attenuation in quartz grains: Archaeometry, v. 21, p. 61–72, doi: 10.1111/j.1475-4754.1979.tb00241.x.

Murray, A., and Wintle, A., 2000, Luminescence dating of quartz using an improved single-aliquot regenerative-dose protocol: Radiation Measurements, v. 32, p. 57–73, doi: 10.1016/S1350-4487(99)00253-X.

Okuda, M., Yasuda, Y., and Setoguchi, T., 2001, Middle to Late Pleistocene vegetation changes at Lake Kopais, Southeast Greece: Boreas, v. 30, p. 73–82, doi: 10.1080/030094801300062347.

Pantosti, D., Martini, P.M.D., Papanastassiou, D., Palyvos, N., Lemeille, F., and Stavrakakis, G., 2001, A reappraisal of the 1894 Atalanti earthquake surface ruptures, central Greece: Bulletin of the Seismological Society of America, v. 91, p. 760–780, doi: 10.1785/0120000051.

Pantosti, D., Martini, P.M.D., Papanastassiou, D., Lemeille, F., Palyvos, N., and Stavrakakis, G., 2004, Paleoseismological trenching across the Atalanti fault (central Greece): Evidence for the ancestors of the 1894 earthquake during the middle ages and roman times: Bulletin of the Seismological Society of America, v. 94, no. 4, p. 531–549, doi: 10.1785/0120020207.

Pirazzoli, P., Stiros, C., Arnold, M., Laborel, J., and Laborel-Deguen, F., 1999, Late Holocene coseismic vertical displacements and tsunami deposits near Kynos, gulf of Euboea, central Greece: Physics and Chemistry of the Earth, v. 24, p. 361–367, doi: 10.1016/S1464-1895(99)00042-3.

Pirazzoli, P.A., Stiros, S.C., Fontugne, M., and Arnold, M., 2004, Holocene and Quaternary uplift in the central part of the southern coast of the Corinth Gulf (Greece): Marine Geology, v. 212, p. 35–44, doi: 10.1016/j.margeo.2004.09.006.

Prescott, J.R., and Hutton, J.T., 1994, Cosmic ray contributions to dose rates for luminescence and ESR dating: Large depths and long-term time variations: Radiation Measurements, v. 23, p. 497–500, doi: 10.1016/1350-4487(94)90086-8.

Reimer, P.J., Baillie, M.G.L., Bard, E., Bayliss, A., Beck, J.W., Bertrand, C.J.H., Blackwell, P.G., Buck, C.E., Burr, G.S., Cutler, K.B., Damon, P.E., Edwards, R.L., Fairbanks, R.G., Friedrich, M., Guilderson, T.P., Hogg, A.G., Hughen, K.A., Kromer, B., McCormac, F.G., Manning, S.W., Ramsey, C.B., Reimer, R.W., Remmele, S., Southon, J.R., Stuiver, M., Talamo, S., Taylor, F.W., van der Plicht, J., and Weyhenmeyer, C.E., 2004, Intcal04 terrestrial radiocarbon age calibration, 26-0 ka bp: Radiocarbon, v. 46, p. 1029–1058.

Smith, A., 1994, Late Quaternary tectonics, sedimentation and sea-level changes in the north Aegean region [Ph.D. thesis]: Cambridge, England, University of Cambridge.

Stein, R.S., and Barrientos, S.E., 1985, Planar high-angle faulting in the basin and range: Geodetic analysis of the 1983 Borah Peak Idaho earthquake: Journal of Geophysical Research, v. 90, p. 11,355–11,366, doi: 10.1029/JB090iB13p11355.

Stiros, S.C., Arnold, M., Pirazzoli, P.A., Laborel, J., Laborel, F., and Papageorgiou, S., 1992, Historical coseismic uplift on Euboea island Greece: Earth and Planetary Science Letters, v. 108, p. 109–117, doi: 10.1016/0012-821X(92)90063-2.

Stuiver, M., and Reimer, P.J., 1993, Extended 14 C database and revised CALIB radiocarbon calibration program: Radiocarbon, v. 35, p. 215–230.

Tzedakis, P.C., Frogley, M.R., Lawson, I.T., Preece, R.C., Cacho, I., and de Abreu, L., 2004, Ecological thresholds and patterns of millenial-scale climate variability: The response of vegetation in Greece during the last glacial period: Geology, v. 32, p. 109–112, doi: 10.1130/G20118.1.

Zimmerman, D.W., 1971, Thermoluminescent dating using fine grains from pottery: Archaeometry, v. 13, p. 29–52, doi: 10.1111/j.1475-4754.1971.tb00028.x.

Manuscript Received 27 August 2009
Revised Manuscript Received 5 April 2010
Manuscript Accepted 22 May 2010